Design of CPW-Fed Triple-Band Two-Port MIMO Antenna Isolated by a Metal Sheet Embedded with U-Shaped Slots

Amit Kumar[1], Jugul Kishor[2], Abha Kumari[3], Pawan Kumar Jaiswal[4], Sudhir Kumar[5]

[1]Department of ECE, NIT Srinagar, Hazratbal-190006, India
[2]Department of ETE, Dayananda Sagar College of Engineering, Bangalore, Karnataka – 560078, India
[3]Department of EE, MIT, Muzaffarpur, Bihar-842003, India
[4]Department of ECE, MIT, Muzaffarpur, Bihar-842003, India
[5]Lead Software Engineer at Capital One Services LLC, Capital One West Creek Campus, Henrico, VA, 23238
E-mail:[1]amit.kumarc210@gmail.com, [2]JugulKishor@gmail.com, [3]kmrabha@gmail.com,[4]pawankumar.jaiswal@gmail.com, [5]ksudhir466vv@gmail.com.
ORCID ID: 10000-0002-1871-8315, 20000-0003-1108-998X, 30000-0001-9153-5956, 40000-0002-3215-9804, 50009-0007-5190-3129 .

ABSTRACT: A novel isolation structure embedded with an array of 4×2 U-shaped slots has been placed between two CPW-fed rectangular patch antennas separated by a distance of 0.35 λ0 to achieve a minimum isolation of 17 dB (>20 dB for the major part). A simple two-port CPW-fed patch antenna, each of dimensions 24×20 mm2, gives a wideband response from 2.22–4.86 GHz. The novel embedded U-shaped slot structure converts this wideband response into a dual-band response, with one ranging from 2.10–3.03 GHz and another from 3.45–4.97 GHz, along with a higher-frequency band from 7.15–7.94 GHz. The higher band has been achieved through improved impedance matching resulting from the introduction of the isolation structure. The proposed MIMO antenna covers the 2.1/2.3/2.6 GHz LTE bands, 2.5/3.5 GHz WiMAX, and 2.45 GHz WLAN, and acts as a receiver for all IEEE C-band and X-band satellite communication. The finished prototype was built on a 50×90×0.8 mm3 FR-4 substrate with an antenna area of 0.22 〖λ〗_0^2. Diversity performances–ECC, DG, MEG, TARC, and CCL have been experimentally verified and presented in this article.

INDEX TERMS CPW-fed, Mutual Coupling, MIMO, Rectangular Patch Antenna (RPA).

I. INTRODUCTION

Higher data rates without sacrificing extra bandwidth are the requirements of new wireless technologies. In wireless communication, long-term evolution (LTE) is the fourth-generation (4G) solution, providing wider bandwidth, higher throughput, and improved handoff capabilities compared to third-generation (3G) networks [1]. LTE wireless devices are expected to operate across a range of frequency bands from 400 MHz to 4 GHz [1]. Implementation of LTE bands using multiple-input-multiple-output (MIMO) antennas will deliver revolutionary results, enabling transmission in rich-scattering environments without sacrificing additional bandwidth at higher bit rates or power compared to a single-input-single-output (SISO) antenna system. The integration of MIMO systems with patch antennas for use in unlicensed bands such as WLAN, WiMAX, C-band, and X-band is a significant advancement in wireless communication. Mutual coupling between the antenna elements of a MIMO system causes amplitude and phase errors. So, designing a multi-band MIMO antenna with high isolation between closely spaced antenna elements is challenging. The CPW feed has an additional advantage of being integrated with solid-state devices.

Many isolation structures have been proposed in the literature to reduce mutual coupling between closely spaced microstrip antennas. Defective ground structures (DGSs) [2–4], single-negative property of Split-Ring Resonator (SRRs) and Complementary-Split-Ring-Resonator (CSRRs) [5, 6], single-negative magnetic metamaterials [7, 8], Electromagnetic Band-Gap (EBG) structures [9], fragmented-type structures [10], modified inter-digital capacitor [11], a unique decoupling structure between PIFAs [12], a resonator between PIFAs [13], a novel ITI-shaped isolation structure [14], etched slits in the ground plane [15], T-shaped slot with a chip capacitor [16], T-shaped isolator [17], two symmetric stepped L-shaped open ground slots [18], diamond-

shaped patterned ground resonator [19], T-shape slot impedance transformer [20] and a folded resonator [21] have been used for achieving better isolation. To achieve multi-bands, slots have been etched in the patch area to create a band-stop, as in [10, 22–24], thereby converting the patch into a multi-band patch antenna.

Our proposed MIMO antenna is a two-port CPW-Fed RPA. A unique isolation structure incorporating an array of 4x2 U-shaped slots achieves a minimum isolation of 17 dB (>20 dB for the majority) between the antenna elements, separated by a C-to-C distance of 0.35 λ0. Due to improved impedance matching, the new isolation structure also transforms a wideband MIMO antenna (2.22–4.86 GHz) into a dual-band MIMO antenna (2.1–3.03 GHz and 3.45–4.97 GHz). The Two-port RPA antenna is fabricated on an FR-4 substrate (εr=4.4, loss tangent=0.025), having dimensions 50×90×0.8 mm3, with an antenna area of 0.22 λ_0^2. The fabricated MIMO antenna is useful for the 2.1/2.3/2.6 GHz LTE bands, 2.5/3.5 GHz WiMAX, and 2.45 GHz WLAN, and also serves as a receiver for all IEEE C-band and X-band satellite communication. Also, our proposed triple-band and wideband MIMO antenna is not disturbed by the strong electromagnetic interference created by the high traffic of 5.5 GHz WiMAX and 5.2/5.8 GHz WLAN.

II. ANTENNA DESIGN PROCESS

The final design of the proposed CPW-fed triple-band MIMO antenna is shown in Fig. 1. The entire simulation work has been carried out on the simulation software CST Microwave Studio. All the design parameters and their values are tabulated in Table 1. The entire design has been fabricated on a commercially available substrate FR-4 (εr=4.4, loss tangent=0.025) with dimensions (L× B) 50×90 mm2, having a thickness of 0.8 mm. Firstly, two RPAs of dimensions (L1× B1) 24×20 mm2 separated by a center-to-center distance of 0.35 λ0 (d1=50mm) along the x-axis are presented in Fig. 1(a), where λ0 is the free space wavelength. The antenna elements are fed with a CPW signal feed line of dimensions (L3× B3) 13×4 mm2. The rectangular ground plane of dimensions (L4× B4) 9.7×12.45 mm2 is present on either side of the CPW-feed line, which helps the monopole antenna to achieve a wideband response ranging from 2.22–4.86 GHz as depicted in Fig. 2.

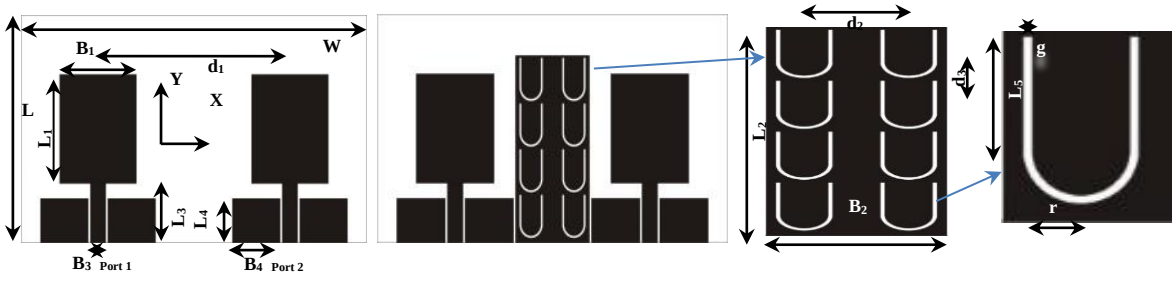

(a) (b) (c) (d)

Fig.1. Design of the proposed MIMO antenna (a) without isolation structure (b) with isolation structure (c) isolation structure (d) Unit U-shaped slot

However, the minimum isolation (|S21|/|S12|) is only 12 dB, which is not good enough to allow our antenna elements to work efficiently with less mutual coupling effect. An isolation structure of dimensions (L2× B2) 41×19 mm2 has been placed between the antenna elements. An array of 4×2 U-shaped slots has been etched on the isolation structure as shown in Fig. 1(c). The U-shaped slots are placed adjacently (center-to-center) at a distance of d2=11 mm, while longitudinally (center-to-center), these are d3=10 mm apart as shown in Fig. 1(c). The dimensions of a single U-shaped slot are shown in Fig. 1(d) and tabulated in Table 1. The width of the etched U-shaped slot is g=0.5mm, and an optimized parameter of the unit U-shaped slot length is L5=7mm with a curvature radius of r=3mm.

Table 1. List of all parameters and their final dimensions

Parameters	**L**	**W**	**L_1**	**L_2**	**L_3**	**L_4**	**L_5**	**B_1**
Unit (mm)	**50**	**90**	**24**	**41**	**13**	**9.7**	**7**	**20**
Parameters	**B_2**	**B_3**	**B_4**	**d_1**	**d_2**	**d_3**	**g**	**r**
Unit (mm)	**19**	**4**	**12.45**	**50**	**11**	**10**	**0.5**	**3**

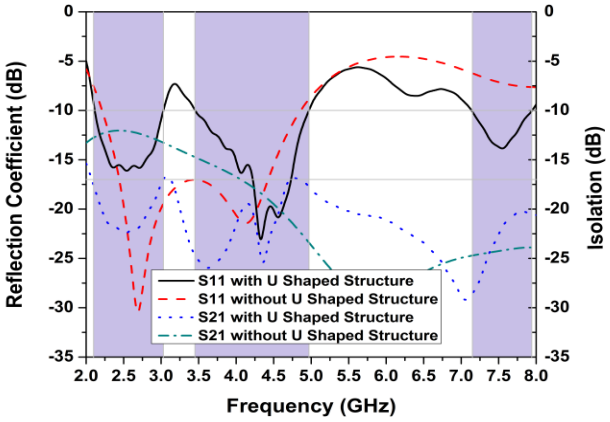

Fig. 2. S-parameters Vs Frequency

The length of the single U-shaped slot has been chosen to resonate at approximately 2.56 GHz, where isolation is very poor. The chosen U-shaped slot structure achieves the required resonant length with less area than other slot structures, such as L- and T-shaped ones. Two columns of U-slots help in canceling the induced current direction, as the direction of current in either column will be 1800 out of phase at any instant of time. Thus, the surface current cannot travel from one antenna element to another, reducing mutual coupling and increasing the minimum isolation by almost 10 dB at 2.56 GHz, bringing it well above 22 dB. The improved isolation (|S21|/|S12|) is clearly visible in Fig. 2, where we can see that the minimum isolation is 17 dB, while it is below 20 dB for the major part of the working frequency band. The isolation characteristics are further strengthened and verified through surface current and E-field distributions at 2.56 GHz, presented in Figs. 3 and 4 after exciting port-1 and terminating the other port-2 with a matched load of 50 Ω. High surface current density can be seen on the second RPA after the excitation of the first patch antenna, which is going to be minimized due to the U-shaped array isolation structure, as clearly shown in Fig. 3. This actually advocates that the isolation structure restricts the propagation of surface current from one patch antenna to another, thus helping in optimizing the antenna efficiency.

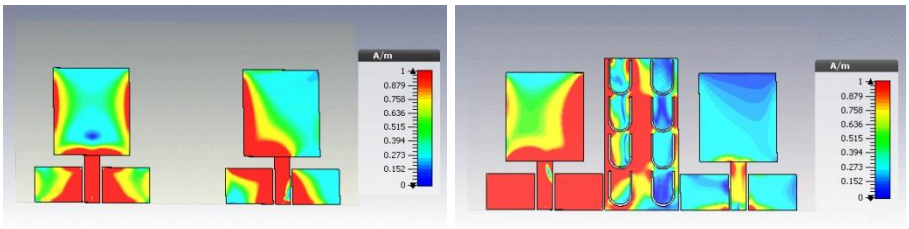

Fig. 3. Surface current distributions at 2.56 GHz

Similarly, the electric field distribution inside the substrate has been significantly reduced in the case of the U-shaped slot isolation structure compared to that without the U-shaped slot isolation structure, as shown in Fig. 4.

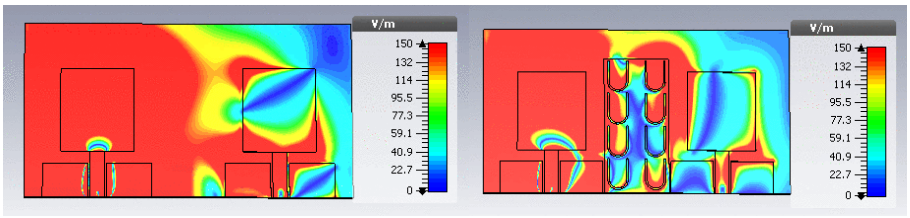

Fig. 4. E-field distribution at 2.56 GHz

The isolation structure has converted the wideband response into a dual-band response with one ranging from 2.1–3.03 GHz and another from 3.47–4.97 GHz. The Lower band suggests compactness in the antenna, making the proposed MIMO antenna usable for the 2.1 GHz LTE band as well. Also, the second band is wide enough to serve as a receiver for all the IEEE C-bands. A third band is achieved from 7.15–7.94 GHz due to improved impedance matching after the introduction of the novel isolation structure. Due to the third band, our proposed antenna will also act as a receiver for the X-band satellite communication.

a. Evolution of the novel Isolation Structure

The evolution of the novel isolation structure from model M.1 to model M.4 is shown in Fig. 5. Their S-parameter analysis is shown in Fig. 6, and the same is tabulated in Table 2. Firstly, a thin metal strip of dimensions 41×0.5 mm^2 has been introduced between the antenna elements, as shown in M.1, as in [14]; however, there is no significant improvement in isolation, as the minimum isolation remains 12 dB.

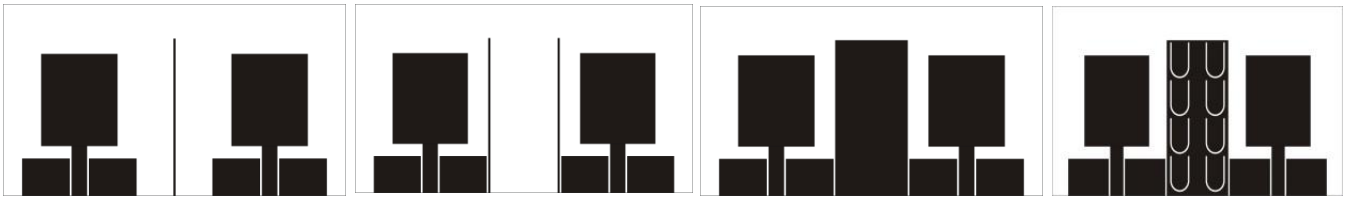

Fig. 5. Evolution design steps from model M.1 to M.4

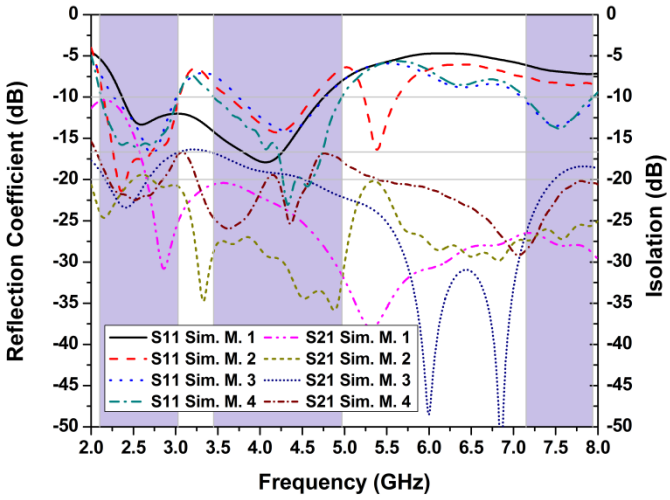

Fig. 6. S-parameter analysis of model M.1 to M.

Table 2. Analysis of models M.1 to M.4

Model No.	-10 dB BW (GHz)	S_{21} (dB)
M.1	2.37–4.76	-12
M.2	2.15–3.04, 3.63–4.63, 5.23–5.63	-20
M.3	2.27–3.00, 3.74–4.77, 7.10–8.00	-17
M.4	2.10–3.03, 3.45–4.97, 7.15–7.94	-17

Now, as in [14], a pair of metal strips of the same dimensions as in model M.1 has been placed, with a spacing of only 0.5 mm from the ground plane of the antenna elements. We can see a significant improvement in isolation, which increased to 20 dB, but the impedance bandwidth is disturbed, resulting in a triple-band. The band gap from 3.04–3.63 GHz resulted in the isolation of the 3.5 GHz WiMAX coverage, while the third band (5.23–5.63 GHz) of model M.2 invites electromagnetic interference from high traffic of 5.5 GHz WiMAX and 5.2 GHz WLAN. To avoid these problems, we have proceeded to M.3, where we have tried to fill the entire area between the metal strips by replacing it with a metal sheet of

dimensions 41×19 mm2, resulting in a triple-band with a minimum isolation of 17 dB. In model M.3, the problem of high traffic on the 5.2 GHz WLAN and 5.5 GHz WiMAX has been removed, but we are unable to cover the 3.5 GHz WiMAX, and the compactness we achieved in model M.2, favoring the 2.1 GHz LTE band, is lost. However, the third band favors the X-band satellite communication, an added advantage. To achieve compactness and improve the impedance bandwidth, U-shaped slots of a 4×2 array have been introduced on the metal sheet, as depicted in model M.4. The slot lengths have been chosen to resonate in the lower frequency band. The resultant triple-band is suitable for the 2.1 GHz LTE band and will also serve for all the IEEE C-bands, incorporating all the benefits of model M.3.

III. RESULTS AND DISCUSSIONS

The final prototype of our proposed CPW-fed triple-band MIMO antenna has been fabricated as shown in Fig. 7. The measured and simulated S-parameters are shown in Fig. 8. The measurements were performed using a two-port Vector Network Analyzer (N5230A). The measured results are in good agreement with the simulated results. We can see the measured isolation is even better than the minimum simulated isolation of 17 dB.

Fig. 7. Fabricated proposed MIMO antenna

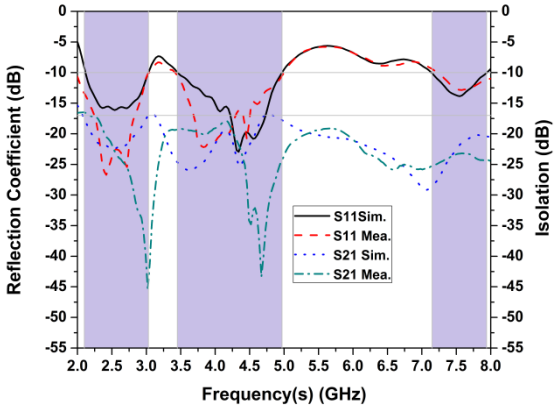

Fig. 8. Simulated and Measured S-parameters analysis of the proposed MIMO antenna

Measured gain and efficiency have been compared with the simulated gain and efficiency after positioning the antenna at theta (θ)=0 and phi (Φ)=0 as presented in Fig. 9. The gain and efficiency are above 0 dB and 75%, respectively, throughout the operating range. The mismatch in the results is due to fabrication limitations and noise in the anechoic chamber during the measurements.

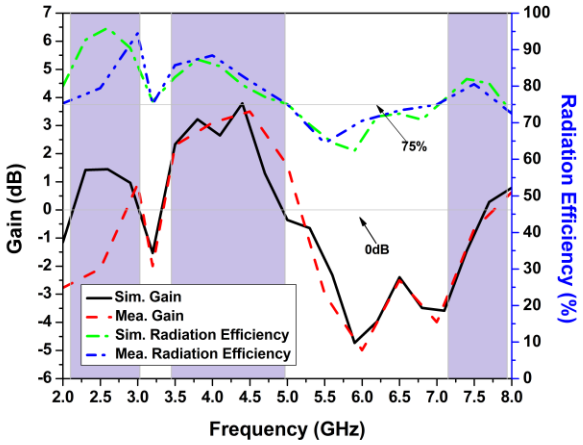

Fig. 9. Gain of the proposed MIMO antenna

Table 3. Comparisons of the proposed Two-port MIMO antenna with the existing MIMO antennas

Ref.	**Size (mm×mm×mm)**	**-10 dB BW (GHz)**	**IBW (Impedance bandwidth)**	**$\|S_{21}\|$ (dB)**	**Dielectric Constant, ε_r**	**Gain (dB/dBi)**	**Efficiency (%)**
Prop.	50×90×0.8 =3600	2.1–3.03 (2.19–2.84), 3.45–4.97 (3.45–4.58), 7.15–7.94	36.3, 36.1%, and 10.5%	17 (mostly >20)	4.4	3.5 dB max	75–90
[1]	50×50×0.8=2000	2.42–2.57	6%	17.3	4.4	0.2418	–
[15]	43×43×1.6=2958.4	2.27–2.35	3.46%	20	2.8	3.66 dBi	88 max.
[16]	90×55×0.8=3960	2.2–2.53	13%	20	4.4	2.2 max	42
[17]	65.25×65.25×1.524=6488.53	2.31–2.51	8.3%	17	4.4	3–3.1	87–91
[18]	44×32×1.6=2252.8	2.6–3.08, 5.42–6.18	16% and 13.1%	21	4.4	3.48 max	–
[19]	72.4×20×0.8=1158.4	2.18–2.65	19.5%	20	3.48	1.04–1.39 dBi	68.2–73.6
[20]	40×90×1.55=5580	2.4–2.78, 3.4–3.6	14.6% and 5.7%	19	4.7	2.4–3.4	77 max.
[21]	75×50×1.6=6000	2.4–2.484	3.27%	18	4.4	1.4	80

To validate the performance and credibility of our proposed MIMO antenna, comparisons have been made with existing two-port MIMO antennas reported in the literature. The comparisons have been shown in Table 3. The comparison chart shows that our MIMO antenna is more compact than many existing two-port antennas, especially in the ISM band at 2.4 GHz. The impedance bandwidth is better than that of any MIMO antenna, with comprehensive isolation of 20 dB (2.19–2.84 & 3.45–4.58), albeit at the cost of some bandwidth, as shown in Table 3. Also, the efficiency exceeds 75% and reaches 90% across the entire working band.

The normalized simulated and measured Co and cross polarization far-field radiation patterns in E-plane (XZ plane) and H-plane (YZ plane) at resonant frequencies 2.56 GHz, 4.22 GHz, and 7.55 GHz are shown in Fig. 10. During measurement, one port is excited, and another port is terminated with a matched load of 50Ω. To reduce ambiguity in the polar plot, the simulated cross-polarization effects of both ports are not shown in the graph. The E-plane shows an almost omnidirectional pattern at each resonant frequency, including both ports. The signal dropout will decrease regardless of the direction of signal arrival, an important objective of MIMO antennas. Also, the antenna is linearly polarized, as we can see an isolation of more than 20 dB in the Co and cross-polarization patterns along the main lobe direction.

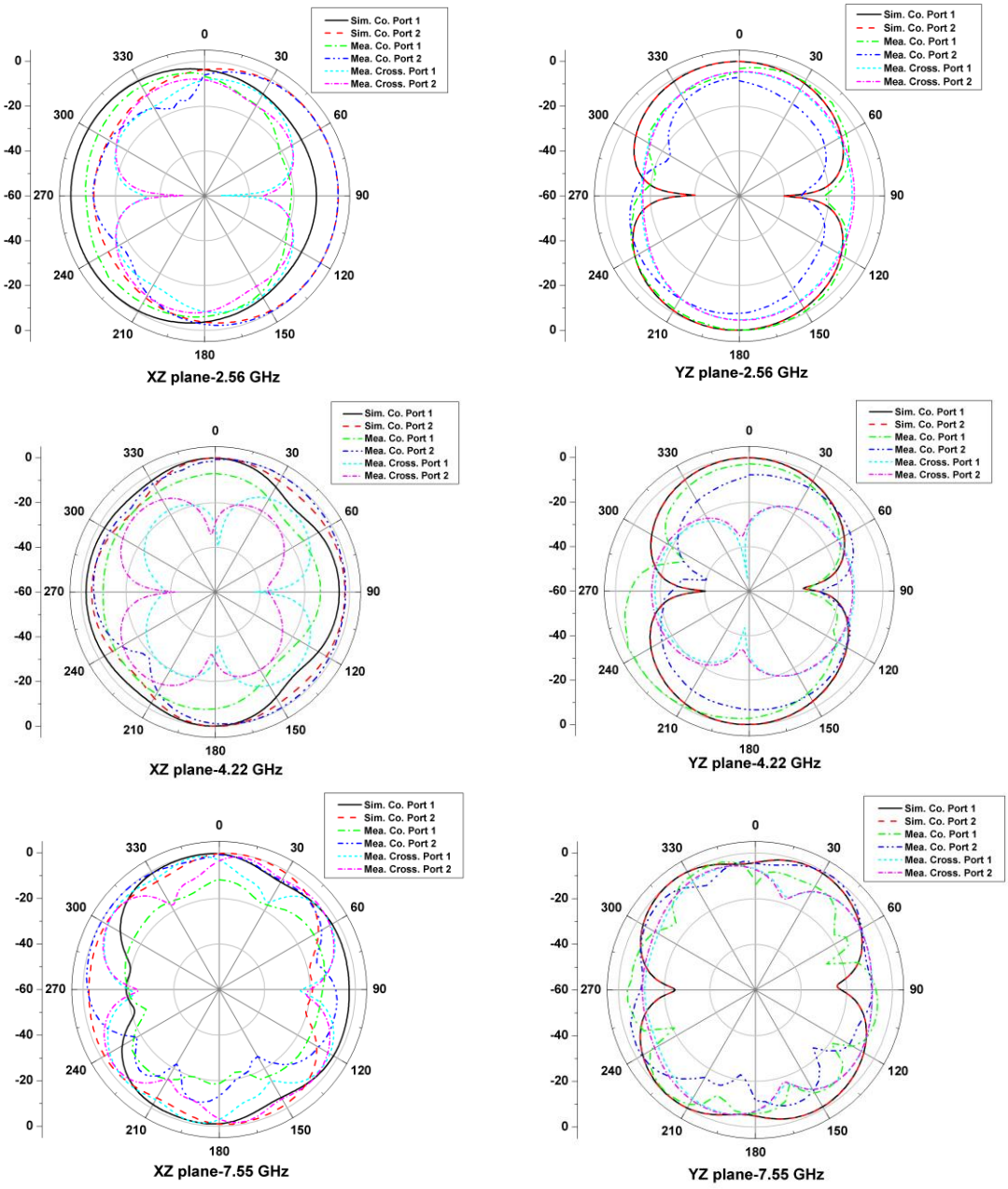

Fig. 10. Normalized radiation pattern

IV. DIVERSITY PERFORMANCES

To validate the performance of the proposed MIMO antenna, some of the diversity performance parameters need to be calculated and experimentally verified. In the discussion shown below, we will be calculating diversity parameters–Envelope correlation coefficient (ECC), Mean effective gain (MEG), Total active reflection coefficient (TARC), and Channel capacity loss (CCL).

a. ECC and DG

The ECC has been computed using equation (1) based on the antenna's far-field radiation pattern [14, 25, 26]. The ECC computed using S-parameters [5, 11, 27] generally yields lower values, whereas analysis of ECC via far-field radiation patterns reveals the true significance of correlation among antenna elements, especially for wideband antennas. The computed ECC is as low as 0.04, as shown in Fig. 11, indicating that the antenna elements are almost unaffected by the far-field radiation

pattern of the other antenna elements, favoring spatial diversity. We have calculated the diversity gain (DG) [14] using equation (2), and the value is 9.95, as shown in Fig. 11.

$$\rho_{ij} = \frac{\left|\int \Omega\left[XPR \cdot E_{\theta i} E_{\theta j}^{*} P_{\theta} + E_{\phi i} E_{\phi j}^{*} P_{\phi}\right] d\Omega\right|^{2}}{\int \Omega\left\{XPR \cdot E_{\theta i} E_{\theta i}^{*} P_{\theta} + E_{\phi i} E_{\phi i}^{*} P_{\phi}\right\} d\Omega \times \int \Omega\left\{XPR \cdot E_{\theta j} E_{\theta j}^{*} P_{\theta} + E_{\phi j} E_{\phi j}^{*} P_{\phi}\right\} d\Omega} \quad (1)$$

$$DG = \sqrt{\left(1 - \left|0.99 \rho_{ij}\right|\right)^{2}} \quad (2)$$

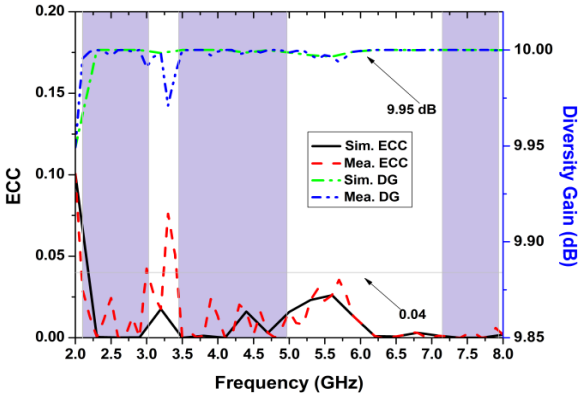

Fig. 11. Simulated and Measured ECC and DG

b. MEG

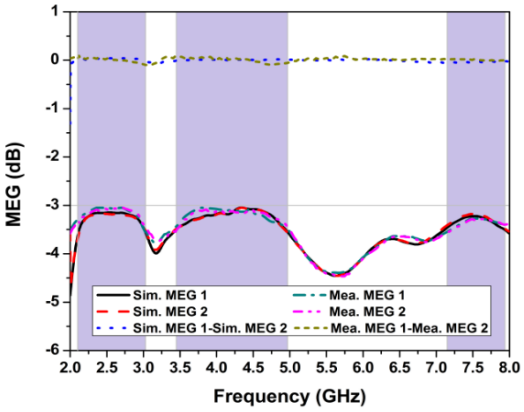

Fig. 12. Simulated and Measured MEG

$$MEG = \int_{0}^{2\pi} \int_{0}^{\pi} \left[\frac{XPR}{1+XPR} G_{\theta}(\theta,\phi) P_{\theta}(\theta,\phi) + \frac{1}{1+XPR} G_{\phi}(\theta,\phi) P_{\phi}(\theta,\phi) \right] \sin\theta d\theta d\phi \quad (3)$$

MEG is the amount of power received by the individual elements of the MIMO antenna in a multipath fading environment as compared to the isotropic antenna. The outdoor environment is considered a uniform Rayleigh environment with equal vertical and horizontal power densities [5]. The MEG is computed using equation (3) [14] and presented in Fig. 12. The MEG is close to -3 dB for the working band and poorer in the non-working zone. Also, the difference in MEG between antenna elements should lie within ±3 dB [5, 14], as shown in Fig. 12.

c. TARC

TARC is defined in terms of the incident and reflected wave powers. This helps in realizing the performance of the MIMO antenna even when the phase [theta (θ)] of the input signal is changing, as shown in Fig. 13. The TARC has been evaluated using equation (4) [3, 11, 14]. It actually indicates that the impedance bandwidth and frequency resonance of the MIMO antenna should not vary with changes in the phase of the input signal. We can see in Fig. 13 that the TARC follows the path of the resultant S-parameter results when the phase of the input signal is held constant at $1e^{j\theta}$ for one port and varied for the other.

$$TARC = \frac{\sqrt{\left|S_{11}+S_{12}e^{j\theta}\right|^2+\left|S_{21}+S_{22}e^{j\theta}\right|^2}}{\sqrt{2}} \quad (4)$$

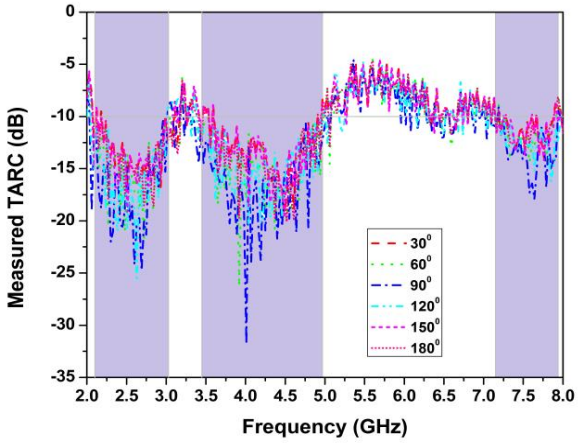

Fig. 13. Computed measured TARC

d. CCL

The CCL assigns accountability for the maximum attainable data transmission rate at which information can be continuously transmitted over the wireless channel with a loss less than 0.4 bits/s/Hz [5, 11, 14]. The CCL has been evaluated using equation (5) [5, 11, 14]. We can see that the CCL is well below the required level, as shown in Fig. 14.

$$C_{loss} = -\log_2 \det\left(\alpha^R\right) \quad (5)$$

where $\alpha^R = \begin{bmatrix} \alpha_{11} & \alpha_{12} \\ \alpha_{21} & \alpha_{22} \end{bmatrix}$ $\alpha_{ii} = 1 - \left(\sum_{j=1}^{N} |S_{ij}|^2\right)$ $\alpha_{ij} = -\left(S_{ii}^* S_{ij} + S_{ji}^* S_{ij}\right)$

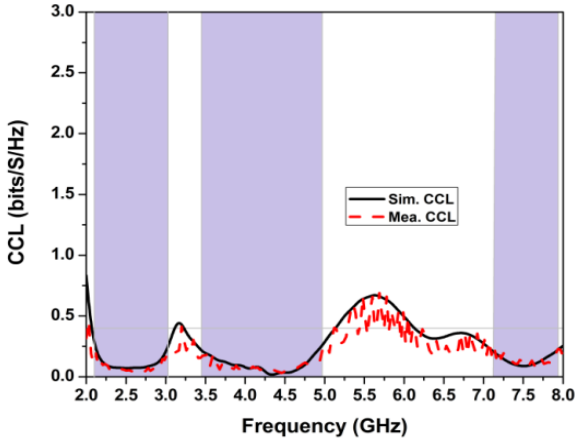

Fig. 14. CCL Vs Frequency

V. CONCLUSIONS

A CPW-fed triple-band two-port MIMO antenna has been presented in this literature. The RPA elements are isolated by introducing a novel isolation structure comprising an array of 4×2 U-shaped etched slots placed between them. The designed MIMO antenna has been fabricated on an FR-4 substrate of dimensions 50×90×0.8 mm^3. A minimum isolation of 17 dB (>20 dB for the majority) has been achieved across all three bands: 2.1–3.03 GHz, 3.45–4.97 GHz, and 7.15–7.94 GHz. The proposed antenna has a maximum gain of 3.5 dB and an efficiency greater than 75% throughout. The antenna has proven diversity performance with ECC < 0.04, CCL < 0.4 bits/S/Hz, and MEG around -3 dB across the entire working range. The MIMO antenna will work in the 2.1/2.3/2.6 GHz LTE bands, 2.5/3.5 GHz WiMAX, and 2.45 GHz WLAN, and will also act as a receiver for all IEEE C-band and X-band satellite communication.

VI. REFERENCES

[1] A. C. J. Malathi, and D. Thiripurasundari, "CSRR Loaded 2×1 Triangular MIMO Antenna for LTE Band Operation," Advanced Electromagnetics 6 (2017), 78-83.

[2] S. S. Jehangir, M. S. Sharawi and A. Shamim, "Highly miniaturised semi-loop meandered dual-band MIMO antenna system," IET Microwaves, Antennas & Propagation, 12 (2018), 864-871.

[3] J. OuYang, F. Yang and Z. M. Wang, "Reducing Mutual Coupling of Closely Spaced Microstrip MIMO Antennas for WLAN Application," IEEE Antennas and Wireless Propagation Letters, 10 (2011), 310-313.

[4] A. B. Numan, M. S. Sharawi, A. Steffes and D. N. Aloi, "A defected ground structure for isolation enhancement in a printed MIMO antenna system," European Conference on Antennas and Propagation (EuCAP), (2013), 2123-2126.

[5] A. Kumar, A. Q. Ansari, B. K. Kanaujia, and J. Kishor, "High Isolation Compact Four-Port MIMO Antenna Loaded with CSRR for Multi-band Applications," Frequenz, 72 (2018), 415-427.

[6] M. S. Khan, A. D. Capobianco, S. M. Asif, D. E. Anagnostou, R. M. Shubair and B. D. Braaten, "A Compact CSRR-Enabled UWB Diversity Antenna," IEEE Antennas and Wireless Propagation Letters, 16 (2017), 808-812.

[7] M. M. Bait-Suwailam, M. S. Boybay and O. M. Ramahi, "Electromagnetic Coupling Reduction in High-Profile Monopole Antennas Using Single-Negative Magnetic Metamaterials for MIMO Applications," IEEE Transactions on Antennas and Propagation, 58 (2010), 2894-2902.

[8] S. R. Thummaluru and R. K. Chaudhary, "Mu-negative metamaterial filter-based isolation technique for MIMO antennas," Electronics Letters, 53 (2017), 644-646.

[9] D. H. Margaret, M. R. Subasree, S. Susithra, S. S. Keerthika and B. Manimegalai, "Mutual coupling reduction in MIMO antenna system using EBG structures," International Conference on Signal Processing and Communications (SPCOM), (2012), 1-5.

[10] L. Wang, G. Wang, and J. Siden, "Design of Fragment-Type Isolation Structures for MIMO Antennas," Progress In Electromagnetics Research C, 52 (2014), 71-82.

[11] A. Kumar, A. Q. Ansari, B. K. Kanaujia, J. Kishor, and N. Tewari, "Design of Triple-Band MIMO Antenna with One Band-Notched Characteristic," Progress In Electromagnetics Research C, 86 (2018), 41-53.

[12] J. H. Xun, L. F. Shi, W. R. Liu, G. X. Liu and S. Chen, "Compact Dual-Band Decoupling Structure for Improving Mutual Coupling of Closely Placed PIFAs," IEEE Antennas and Wireless Propagation Letters, 16 (2017), 1985-1989.

[13] L. Minz and R. Garg, "Reduction of mutual coupling between closely spaced PIFAs," Electronics Letters, 46 (2010), 392-394.

[14] A. Kumar, A. Quaiyum Ansari, B. Kumar Kanaujia, and J. Kishor, "A Novel ITI-Shaped Isolation Structure Placed Between Two-Port CPW-Fed Dual-Band MIMO Antenna for High Isolation," AEU - International Journal of Electronics and Communications, 104 (2019), 35-43.

[15] C. Chiu, C. Cheng, R. D. Murch and C. R. Rowell, "Reduction of Mutual Coupling Between Closely-Packed Antenna Elements," IEEE Transactions on Antennas and Propagation, 55 (2007), 1732-1738.

[16] J. Park, J. Choi, J. Park and Y. Kim, "Study of a T-Shaped Slot With a Capacitor for High Isolation Between MIMO Antennas," IEEE Antennas and Wireless Propagation Letters, 11 (2012), 1541-1544.

[17] L. Malviya, R. K. Panigrahi, and M. V. Kartikeyan, "2x2 MIMO antenna for ISM band application," 11th International conference on Industrial and Information Systems (ICIIS), (2016), 794-797.

[18] S. P. Biswal and S. Das, "Two-element printed PIFA-MIMO antenna system for WiMAX and WLAN applications," IET Microwaves, Antennas & Propagation, 12 (2018), 2262-2270.

[19] D. Wu, S. W. Cheung, Q. L. Li and T. I. Yuk, "Decoupling using diamond-shaped patterned ground resonator for small MIMO antennas," IET Microwaves, Antennas & Propagation, 11 (2017), 177-183.

[20] S. Zhang, B. K. Lau, Y. Tan, Z. Ying and S. He, "Mutual Coupling Reduction of Two PIFAs With a T-Shape Slot Impedance Transformer for MIMO Mobile Terminals," IEEE Transactions on Antennas and Propagation, 60 (2012), 1521-1531.

[21] C. Lee, S. Chen and P. Hsu, "Integrated Dual Planar Inverted-F Antenna With Enhanced Isolation," IEEE Antennas and Wireless Propagation Letters, 8 (2009), 963-965.

[22] H. W. Liu, C. H. Ku and C. F. Yang, "Novel CPW-Fed Planar Monopole Antenna for WiMAX/WLAN Applications," IEEE Antennas and Wireless Propagation Letters, 9 (2010), 240-243.

[23] R. Pandeeswari and S. Raghavan, "A CPW-Fed triple band OCSRR embedded monopole antenna with modified ground for WLAN and WiMAX applications," Microw. Opt. Technol. Lett., 57 (2015), 2413–2418.

[24] F. Yu and C. Wang, "Design of a CPW-fed Dual Band-Notched Planar Wideband Antenna for UWB Applications," Ultra Wideband Communications Mohammad Abdul Matin, IntechOpen, (2011) 239-254.

[25] A. Kumar, A. Q. Ansari, B. K. Kanaujia, J. Kishor, and P. Kandpal, "Design of CPW-Fed Triple-Band Two-Port MIMO Antenna with U-Shaped Slot Isolation Structure for High Isolation," IEEE International Microwave and RF Conference (IMaRC), (2018).

[26] A. Kumar, G. Saxena, P. Kumar, Y. K. Awasthi, P. Jain, S. S. Singhwal and P. Ranjan, "Quad-Band Circularly Polarized Super-wideband MIMO Antenna for Wireless Applications," International Journal of RF and Microwave Computer-Aided Engineering, vol. 32, no. 06, e23129, June 2022.

[27] M. -A. Chung, M. -C. Hsieh, C. -C. Hsu and C. -W. Lin, "A Compact Multi-Band MIMO Antenna With High Isolation and Low SAR for LTE and Sub-6 GHz Applications," in IEEE Access, vol. 13, pp. 46014-46029, 2025.